# JFM RAPIDS
journals.cambridge.org/rapids

# Motion of Newtonian drops deposited on liquid-impregnated surfaces induced by vertical vibrations

**Paolo Sartori**[1], **Elia Guglielmin**[1], **Davide Ferraro**[1], **Daniele Filippi**[1], **Annamaria Zaltron**[1], **Matteo Pierno**[1] and **Giampaolo Mistura**[1,†]

[1]Dipartimento di Fisica e Astronomia 'G. Galilei', Università di Padova, via Marzolo 8, 35131 Padova, Italy

We have studied the motion of drops on inclined liquid-impregnated surfaces (LISs) subject to vertical vibrations. The liquid drops comprise distilled water and different aqueous solutions of glycerol of increasing viscosity. The use of weak pinning LISs strongly affects the dynamical phase diagram. First of all, there is no trace of the dominant static region at low oscillating amplitudes reported for oscillating solid surfaces characterized by contact angle hysteresis. On the contrary, at sufficiently low oscillating amplitudes, the drops always move downwards with a velocity that depends only on the drop viscosity. Further increasing the oscillating amplitude may drive the drop upwards against gravity, as reported for dry surfaces. The use of more viscous drops widens this climbing region. Arguably, the main novelty of this work concerns the observation of two distinct descending regimes where the downhill speed differs by a factor of five or more. Fast-rate videos show that the evolution of the drop profile is diverse in the two regimes, likely because the vertical oscillations reduce the effect of the oil meniscus surrounding the drop at high accelerations.

**Key words:** drops, contact lines, microfluidics

## 1. Introduction

Controlling the motion of liquid drops in contact with a solid surface has broad technological implications in many different areas, ranging from textiles to microfluidics and heat exchangers (Mistura & Pierno 2017). This control can be achieved in a passive way by decorating the surface with suitable chemical traces (Suzuki *et al.* 2008; Nakajima *et al.* 2013; Liu & Xu 2015; Zhao, Chen & Liu 2016, 2017; Lin *et al.* 2018). The presence of domains of different wettability introduces interfacial forces that affect the droplet dynamics (Bonn *et al.* 2009). For instance,

† Email address for correspondence: giampaolo.mistura@unipd.it

parallel stripes can slow down (Sbragaglia *et al.* 2014), deviate (Semprebon *et al.* 2016) or induce nonlinearities (Varagnolo *et al.* 2013) in the drop motion. If the pattern is not symmetric, like an array of triangular domains (Varagnolo *et al.* 2014), the motion can be anisotropic. Active control on functionalized surfaces can be instead realized with a variety of external stimuli, which include electric (Mugele & Baret 2005) and magnetic (Latikka *et al.* 2018; Rigoni *et al.* 2018) fields, light (Dattilo *et al.* 2007; Banerjee, Dionysiou & Pillai 2015), temperature (Darhuber *et al.* 2003) and acoustic vibrations (Yeo & Friend 2014).

The main advantage of using vibrations is that they couple with the liquids inertia; thus they do not require specific material properties. Drops on a horizontal plate vibrating tangentially can unpin from surface defects and move (Daniel & Chaudhury 2002; Daniel *et al.* 2004). If the plate vibrates parallel to gravity, the contact line oscillations are rectified by hysteresis, thus inducing a ratcheting motion to the water drop vertically downwards (Dong, Chaudhury & Chaudhury 2006). Surprisingly, drops on an inclined plane subject to sufficiently strong vertical vibrations can climb against gravity (Brunet, Eggers & Deegan 2007, 2009), regardless of the liquid viscosity and surface wettability (Sartori *et al.* 2015). An extension of this study shows that drops can be moved on a flat surface by simultaneous vertical and horizontal vibrations that are phase-shifted (Noblin, Kofman & Celestini 2009). These intriguing drop behaviours are generally due to the classic ratchet mechanism, i.e. a locally asymmetric but globally symmetric system may induce global transport (Ding *et al.* 2018). In the climbing experiments (Brunet *et al.* 2007, 2009; Sartori *et al.* 2015), the asymmetry is induced by the inclination of the plate with respect to the acceleration (Ding *et al.* 2018). There have been several attempts to model and understand the experimental observation (Brunet *et al.* 2007, 2009; Sartori *et al.* 2015) of climbing motion of droplets using a wide range of assumptions and approximations (see, for example, the summary reported by Bradshaw & Billingham (2018)). Generally, it has been qualitatively attributed to the nonlinear interaction between the drop deformation and the components of the acceleration (Brunet *et al.* 2007; John & Thiele 2010; Benilov & Billingham 2011; Savva & Kalliadasis 2013, 2014; Sartori *et al.* 2015; Bradshaw & Billingham 2016). Recent three-dimensional numerical simulations suggest that the ratchet mechanism is due to a hysteresis of the wetted area in one period of harmonic vibration (Ding *et al.* 2018). In particular, the average wetted area in the downhill stage is larger than that in the uphill stage, which is found to be responsible for the uphill net motion of the drop.

The published experimental studies on the drop climbing of oscillating wedges use solid surfaces characterized by a pronounced contact angle hysteresis $\Delta\theta$ (Brunet *et al.* 2007, 2009; Sartori *et al.* 2015). To shed more light on this fascinating phenomenon, we have systematically studied the dynamics of liquid drops on liquid-impregnated surfaces (LISs) which exhibit negligible hysteresis (for example, $\Delta\theta < 5°$). Newtonian solutions of different viscosities and surface tensions have been investigated. Lack of a static region where the drop is pinned to the vibrating surface, and novel dynamic phases have been observed.

## 2. Methods

### 2.1. *Experimental set-up*

The set-up resembles that used in our previous study of oscillating Newtonian drops (Sartori *et al.* 2015). Drops are deposited on a substrate fixed to an aluminium wedge with an inclination angle $\alpha = 45°$, which is screwed to the moving shaft
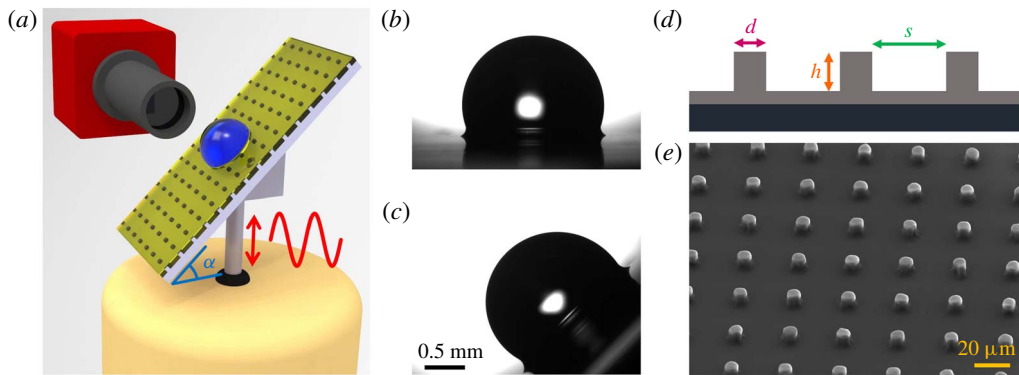
FIGURE 1. (*a*) Schematic drawing of the experimental set-up. Liquid drops are deposited on a LIS attached to an aluminium wedge with an inclination angle $\alpha = 45°$. The wedge is screwed to the shaft of a shaker whose oscillating amplitude and frequency can be accurately controlled. (*b,c*) Photographs of the drop profile on the horizontal (*b*) and inclined (*c*) LIS. (*d*) Characteristic geometry of the surface patterns used for the lubricant impregnation. Films of SU-8 are deposited on silicon wafers and patterned by photolithography. (*e*) SEM image showing a portion of the surface used in this study.

of an electromagnetic shaker, as shown in the schematic diagram of figure 1. The shaker oscillates vertically in the frequency range 10 Hz–10 kHz and the maximum force it can exert is 8.9 N. The vibration amplitude $A$ is determined with an IR phototransistor that is calibrated by optically measuring the net displacement of the shaft (Sartori *et al.* 2018). The resolution in $A$ is estimated to be 2 µm. The vertical acceleration is calculated from the formula $a = 4\pi^2 f^2 A$, where $f$ is the vibrating frequency. With a feedback circuit, it is also possible to sweep $f$ while maintaining $A$ constant over a frequency interval 50–500 Hz.

The drop is illuminated by a backlight LED source. The drop profile is viewed with different cameras and objectives to take spatial and/or temporal high-resolution videos. The profile of each image is then analysed offline by a custom-written program, which yields the apparent contact angles and other relevant geometric quantities (Tóth *et al.* 2011). Special care has been devoted to the removal of spurious resonances caused by the mismatch of the wedge mass centre from the shaker axis. To balance the wedge on the axis, tiny weights are added close to the shaft. The adjustments have been monitored by analysing the line shape of the IR photodetector and taking high-resolution videos of the oscillating shaft. As a result, we are confident that the shaker induces only vertical oscillations up to the maximum accelerations.

## 2.2. *Liquid impregnated surfaces*

Robust omniphobic surfaces can be obtained by trapping a lubricating liquid inside a texture and choosing this liquid to allow a drop of another non-miscible liquid to float on this mixed substrate (Lafuma & Quéré 2011; Wong *et al.* 2011; Mistura & Pierno 2017). The surfaces for our study are prepared in a clean room by using standard photolithography. Silicon wafers are spin-coated with a SU-8 negative photoresist layer of thickness $h$ and exposed to UV light using masks presenting circles of diameter $d$ separated by a distance $s$ (see figure 1). To favour impregnation by a fluorinated oil, the surfaces are silanized with tricloro(1H, 1H,

| Liquid | Concentration (w/w) | Density $\rho$ (g ml$^{-1}$) | Viscosity $\mu$ (mPa s) | Surface tension $\sigma$ (mM m$^{-1}$) |
|---|---|---|---|---|
| Water | Pure | 0.998 | 1.00 | 72.8 |
| | 50 % | 1.126 | 6.0 | 68.6 |
| | 70 % | 1.181 | 23.1 | 66.5 |
| Glycerol/water | 80 % | 1.208 | 60.9 | 65.4 |
| | 95 % | 1.248 | 515 | 63.8 |
| Fomblin Y LVAC 06/6 | Pure | 1.88 | 120 | 21 |

TABLE 1. Main physical properties at 20 °C of the liquids considered in this study (Glycerine Producers' Association 1963; Solvay 2017).

2H, 2H-perfluorooctyl)silane by vapour deposition. The lubricant is a fluorinated oil (Fomblin PFPE (Perfluoropolyether) Y LVAC 06/6, Solvay) with viscosity $\mu_{oil} = 120$ mPa s and surface tension $\gamma_{oil} = 21$ mN m$^{-1}$ at $T = 20$ °C (Solvay 2017). Fluorinated oil completely wets silanized silicon and photoresist. Impregnation is achieved by dip-coating the sample at low velocity (lower than 2 mm s$^{-1}$) from a bath of oil and checking under a microscope that the patterned surface is not over-impregnated with oil. We have explored different patterns. Here we present the results obtained with surfaces patterned by cylindrical posts having $h = 8$ µm and $d = 7$ µm separated by $s = 23$ µm, which we have found to present a long lifetime (longer than two days) and very low contact angle hysteresis ($\Delta\theta < 5°$). The patterned areas have a typical width of 1 cm and a length of 3 cm.

### 2.3. *Liquid solutions*

Drops of known volume are deposited with a syringe pump (UltraMicroPump UMP3, WPI) at the centre of the surface. Besides distilled water, we have also studied different Newtonian, aqueous solutions of glycerol. The main physical parameters of the various aqueous solutions are listed in table 1. The values of density $\rho$, viscosity $\mu$ and surface tension $\sigma$ refer to the working temperature of 20 °C and have been deduced from literature (Glycerine Producers' Association 1963). The corresponding spreading coefficient $S_{ow(a)} = \sigma_{wa} - \sigma_{wo} - \sigma_{oa}$, where $\sigma$ is the interfacial tension between the two phases designated by subscripts $w$ (drop aqueous solution), $o$ (lubricant) and $a$ (air), is greater than zero, implying that the oil cloaks the water drop (Smith *et al.* 2013) with a film of nanometric thickness (Schellenberger *et al.* 2015).

Figure 1 displays two characteristic images of water drops deposited on a horizontal and an inclined LIS. They show that drops are quasi-hemispherical and surrounded by a small oil meniscus. This circular meniscus is pulled from the oil film by the vertical component of the surface tension of water (Smith *et al.* 2013). The side views display an apparent contact angle of approximately 90° and negligible difference between the front and rear contact angles of the moving drop, an indication that the contact angle hysteresis on the LIS is very small.

## 3. Results and analysis

The motion of a liquid drop is found to depend on the acceleration $a$ and the frequency $f$ of the vertical vibrations. Figure 2 displays the dynamical phase diagram
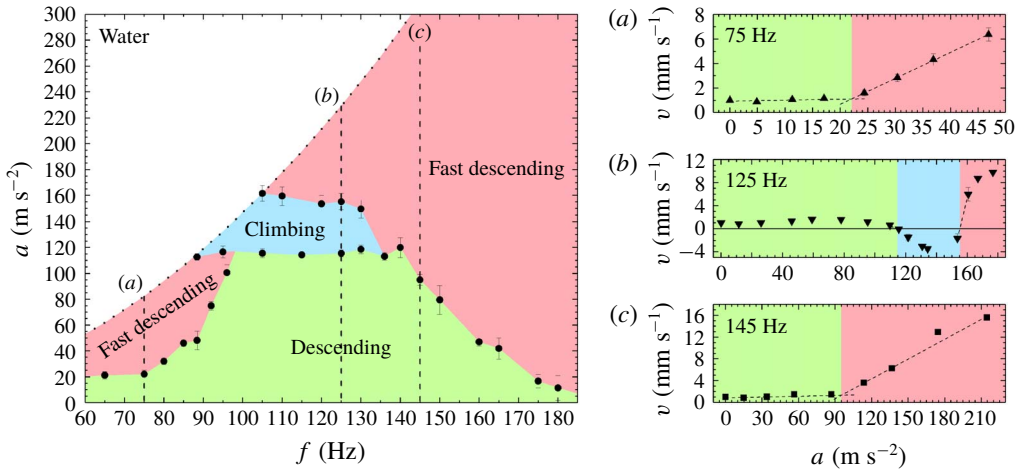
FIGURE 2. Dynamical phase diagram of water drops of volume $\Omega = 1$ µl deposited on a LIS tilted by $\alpha = 45°$. Drop velocity along the acceleration scans at constant frequency (*a–c*) is reported in the side panels.

of pure water drops of volume $\Omega = 1$ µl obtained by scanning, at different constant frequencies, the vertical acceleration. At such small volume, the interfacial tension contribution is dominant and no breakup of the drops is observed (Brunet *et al.* 2007). At variance with our previous work (Sartori *et al.* 2015), we have not normalized these data to the resonance frequency of the drops rocking mode, corresponding to a supported drop vibrated in a direction parallel to the substrate, because all the data we present refer to the same $\Omega = 1$ µl and the liquids have very similar surface tensions and contact angles. Again, the parabolic dashed line separating the upper white region represents the acceleration corresponding to the maximum oscillating amplitude of approximately 0.8 mm provided by our set-up.

A noticeable difference with respect to the original phase diagram measured on Poly(methyl methacrylate) (PMMA) surfaces (Sartori *et al.* 2015) is the absence of a static region where the drop is not moving at low accelerations. The disappearance of this region is a direct consequence of the very low contact angle hysteresis of water drops on LISs, in agreement with numerical calculations (Sartori *et al.* 2015). In analogy with previous experiments (Brunet *et al.* 2007, 2009; Sartori *et al.* 2015), the diagram presents a narrow region where the water drops climb the wedge against gravity with a velocity which can be as high as 5 mm s$^{-1}$, whose existence has been found also in numerical simulations (John & Thiele 2010; Benilov & Billingham 2011; Savva & Kalliadasis 2013, 2014; Bradshaw & Billingham 2016, 2018; Ding *et al.* 2018). The value of the climbing velocity is of the same order as that experimentally observed, although a quantitative comparison with previous studies is not possible because they considered different inclination angles, volumes and viscosities (Brunet *et al.* 2007, 2009; Sartori *et al.* 2015).

Arguably, the novel feature of this phase diagram is the presence of two distinct descending regions (see red and green zones in figure 2). The boundaries between them can be identified by looking at the characteristic amplitude scans shown in the side panels of figure 2. At fixed increasing amplitudes, water drops are repeatedly deposited on the oscillating substrate and their motion is recorded. The average of the resulting speeds corresponding to at least five runs is then plotted in the amplitude

**876** R4-5

scans. To make sure that the data are not affected by an irreversible modification in the system, at the end of any amplitude scan the shaker is turned off and the new velocity is compared with the initial one. In all the scans we present, the final velocity coincides with the initial one within the statistical error.

Scan (*a*) at $f = 75$ Hz initially presents a constant downward (assumed positive) velocity of approximately 1 mm s$^{-1}$, a value consistent with those measured on static LISs with similar inclinations and oil viscosity (Smith *et al.* 2013; Keiser *et al.* 2017; Rigoni *et al.* 2018). Above $a \sim 22$ m s$^{-2}$, a linear increase in the downward velocity is observed. We point out that this boundary does not signal any variation in the downhill dynamics, which remains characterized by a constant velocity typical of viscous motion. Scan (*b*) at $f = 125$ Hz initially exhibits the same constant downward velocity of approximately 1 mm s$^{-1}$, then at $a \sim 115$ m s$^{-2}$ the drop stops and starts moving upwards at increasing speed, till at $a \sim 155$ m s$^{-2}$ the drop reverses direction and starts moving downwards at much higher velocities, close to 10 mm s$^{-1}$. The maximum climbing speed observed, approximately 4 mm s$^{-1}$, is similar to that originally measured on a PMMA surface with the same inclination of 45°, but characterized by a contact angle hysteresis $\Delta\theta = 33°$ (Brunet *et al.* 2007), although a more quantitative comparison is impossible because the drops have different volume and viscosity. Finally, scan (*c*) at $f = 145$ Hz resembles scan (*a*), namely an initial downward velocity of approximately 1 mm s$^{-1}$, followed by a pronounced increase in the downward velocity above $a \sim 95$ mm s$^{-2}$. Movie 1 available as supplementary material at https://doi.org/10.1017/jfm.2019.600 shows the characteristic drop motion in the different regions.

With a fast camera we have analysed the drop evolution at different stages of the amplitude scan. Figure 3 shows a sequence of side view snapshots taken over an oscillating period (see also movie 2 in supplementary material). They clearly show that the instantaneous drop profile varies significantly between descending and fast descending. A fast descending drop experiences a larger variation in the profile: the peak becomes sharper (see timepoints E and F) and the bump is wider and shallower (see timepoint A and B). Interestingly, the profile evolution of a climbing drop resembles that of a fast descending drop. No transitions to a fast descending regime are observed on a solid surface (Brunet *et al.* 2007, 2009; Sartori *et al.* 2015), suggesting that they may be related to the use of LISs. Actually, when oil is more viscous than the liquid drop, dissipation is expected to take place in oil – that is, in the underlying film and in the surrounding meniscus. A detailed analysis indicates that the resulting friction is caused by viscous effects in the front edge of the moving meniscus surrounding the drop, which determine a nonlinear dependence of the drop velocity with the driving force. As the driving force is increased, the wedge dissipation is suddenly suppressed, which leads to a faster dynamical regime that seems to arise from the self-lubrication of the drop (Keiser *et al.* 2017). Further experiments combined with numerical calculations are required to better elucidate the link of these mechanisms to the observed dynamics of oscillating drops. To better quantify the differences in the snapshots, the graphs in figure 3(*b*) display the periodic variation of the length $\ell$ of the contact area along the direction of the motion for the same three characteristic cases. They show that the variation in $\ell$ increases with the oscillating amplitude. More interesting, there is a marked difference in the phase between $\ell$ and the oscillating amplitude: in the fast descending regime they are practically in phase, while in the descending one they are out of phase by almost 180°.

We have extended these measurements to aqueous solutions of glycerol of increasing viscosity. The results are summarized in the three phase diagrams shown in
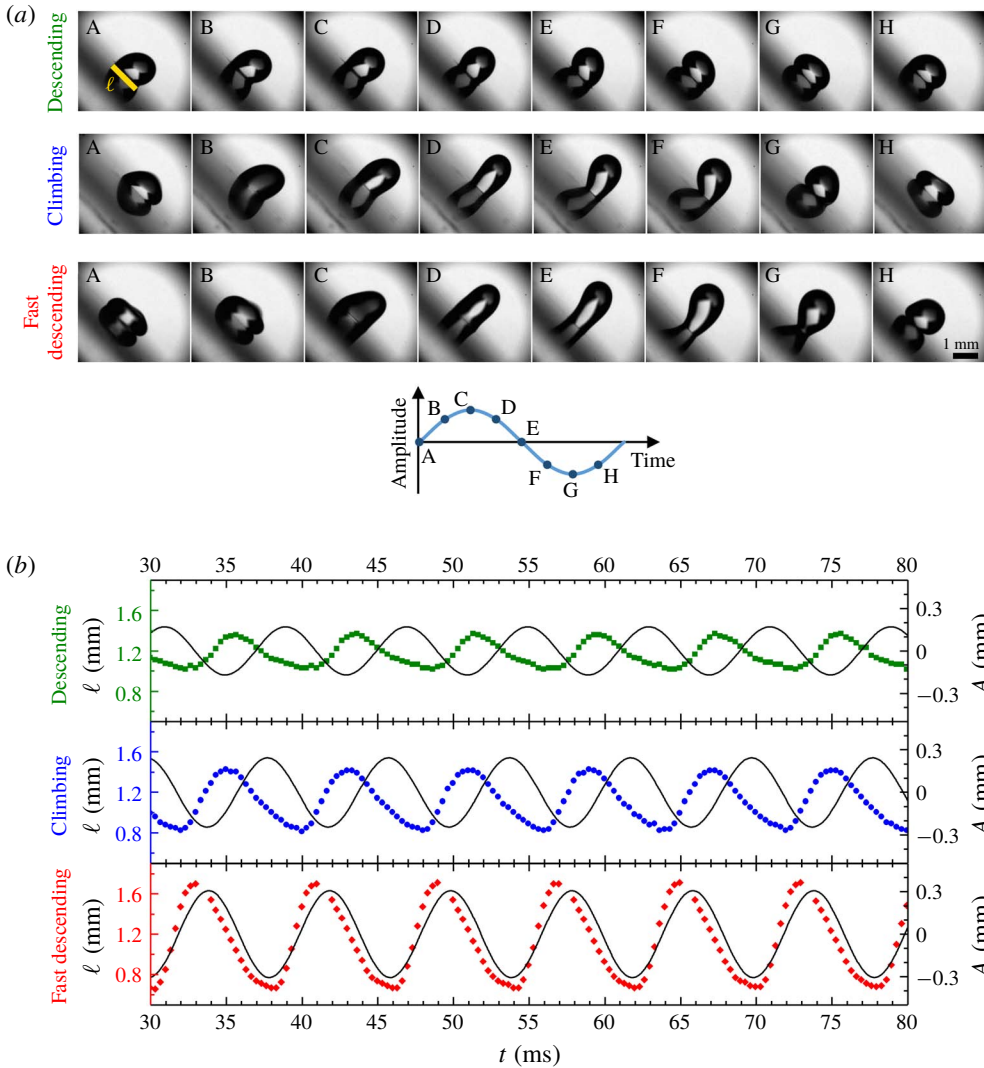
FIGURE 3. (*a*) Side views of a water drop in the 'descending', 'climbing' and 'fast descending' dynamical phases, taken at different instants of a vibrating cycle of frequency $f = 125$ Hz, as indicated in the diagram below the photos from A to H. The accelerations are 105 m s$^{-2}$, 150 m s$^{-2}$ and 190 m s$^{-2}$, respectively. The scale bar is 1 mm. (*b*) Temporal variations of length $\ell$ of the contact area for the three different cases. The length $\ell$ is graphically indicated in the first side view by a yellow bar. The solid lines in the graphs indicate the oscillations in the vertical amplitude $A$ of the substrate.

figure 4. The water diagram is added to facilitate the comparison. The main feature is a pronounced widening of the climbing region at the expense of the fast descending region as the drop viscosity increases. For the most concentrated glycerol solution, the phase diagram essentially consists of a descending region at low accelerations and a climbing region at high accelerations. Sweeping the accelerations between these extremes causes the drop to repeatedly move up and down.
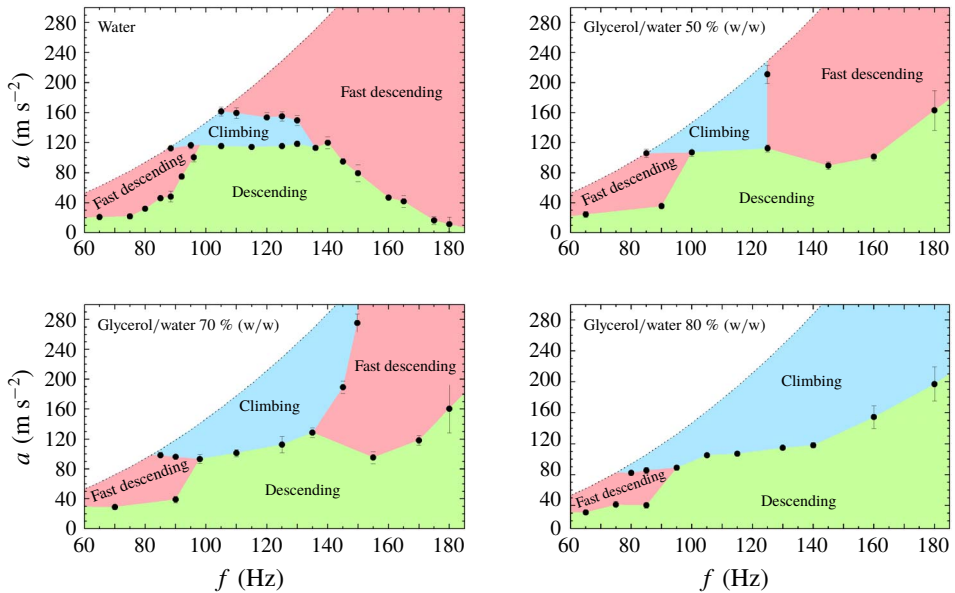
FIGURE 4. Dynamical phase diagrams of drops of different aqueous solutions corresponding to $\Omega = 1$ µl and $\alpha = 45°$.

Figure 5 shows the dependence of the drop velocity on the vertical acceleration for a fixed frequency $f = 100$ Hz and for drops of volume $\Omega = 2$ µl having different viscosity. The drops all have volume $\Omega = 2$ µl to guarantee reliable dosing also for the highly concentrated (95 % (w/w)) glycerol solution, which is more viscous than the lubricant (see table 1). At low $a$ (see inset), the velocity of water drops is approximately 2 mm s$^{-1}$. Similar values are observed with glycerol aqueous solutions up to 80 % (w/w). Instead, drops of almost pure (95 % (w/w)) glycerol solutions move at a velocity of 1 mm s$^{-1}$. These data confirm that two regimes are successively followed by increasing the drop viscosity $\mu$ (Keiser *et al.* 2017): firstly ($\mu < \mu_{oil}$), the speed $v$ plateaus at a value roughly independent of $\mu$, and dissipation mainly occurs in the lubricant; at larger drop viscosity ($\mu > \mu_{oil}$), the speed decreases with $\mu$, indicating that in this regime the dissipation occurs in the drop.

As we increase the vertical acceleration, different trends are observed depending on the drop viscosity. For pure water drops, the downhill speed increases almost linearly with $a$, reaching a value of approximately 30 mm s$^{-1}$ when $a = 160$ m s$^{-2}$. Drops of glycerol solution 70 % (w/w) initially behave as water drops, but, for $a > 30$ m s$^{-2}$, $v$ reaches a plateau around 8 mm s$^{-1}$. Further increasing $a$ causes the drops to slow down till they stop around 120 m s$^{-2}$ and then climb uphill against gravity: when $a = 160$ m s$^{-2}$, the uphill speed amounts to approximately 10 mm s$^{-1}$. The same trend is exhibited by the more viscous drops of glycerol solution 80 % (w/w), the only differences being quantitative: the plateau velocity is much smaller, approximately 2 mm s$^{-1}$, and the drops stop at a lower acceleration, approximately 100 m s$^{-2}$, further suggesting that in this regime the dissipation occurs mainly in the drop. Notably, these drops climb faster: when $a = 160$ m s$^{-2}$, the uphill speed amounts to approximately 15 mm s$^{-1}$. Conversely, the dynamics of drops of almost pure glycerol solution (95 % (w/w)) is significantly hampered and
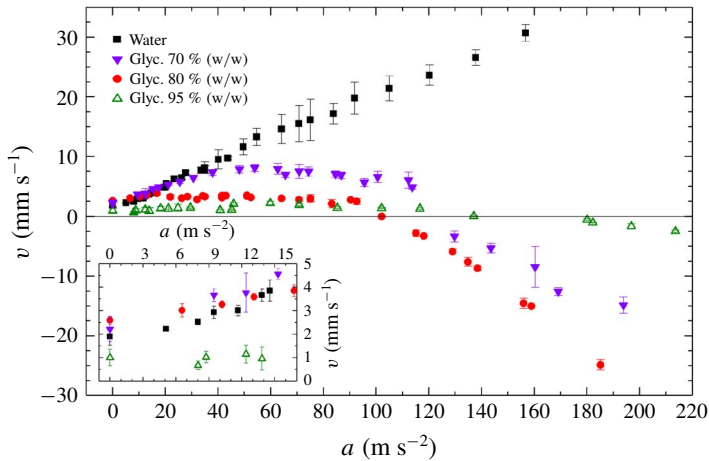
**876** R4-8

FIGURE 5. Velocity of drops of liquid solutions having different viscosity as a function of the vertical acceleration of the post. The inset displays an enlargement of the data at low accelerations. The data refer to drops of volume $\Omega = 2$ µl and an oscillating frequency $f = 100$ Hz.

the maximum speed, either downhill or uphill, remains below 2 mm s$^{-1}$, up to the maximum acceleration achievable with our set-up.

## 4. Conclusions

In conclusion, we have systematically studied the dynamics of Newtonian drops on LISs inclined by 45° and subject to vertical vibrations. The liquids comprise distilled water and different aqueous solutions of glycerol of increasing viscosity. LISs are made by standard lithographic techniques and, to avoid problems with contaminations, measurements are repeated with fresh surfaces which exhibit $\Delta\theta < 5°$. The resulting dynamical phase diagrams are strongly affected by the use of weak pinning LISs. First of all, the drops are always found to descend, even at the lowest oscillating amplitudes, in agreement with theoretical studies of ideal flat surfaces with $\Delta\theta = 0°$. Further increasing the oscillating amplitude may drive the drop upwards against gravity, as reported in previous studies. The use of more viscous drops widens this climbing region. Increasing the amplitude may also induce a new descending regime where the downhill speed is higher by a factor of five or more. Fast-rate videos show that the evolution of the drop profile is diverse in the two regimes, probably because the vertical oscillations reduce the effect of the oil meniscus surrounding the drop at high accelerations. We hope that this preliminary work will stimulate further studies on this system that, despite its simplicity, exhibits quite unexpected dynamical regimes.

## Acknowledgements

## Supplementary movies

Supplementary movies are available at https://doi.org/10.1017/jfm.2019.600.

# References

BANERJEE, S., DIONYSIOU, D. D. & PILLAI, S. C. 2015 Self-cleaning applications of TiO$_2$ by photo-induced hydrophilicity and photocatalysis. *Applied Catal.* B **176**, 396–428.

BENILOV, E. S. & BILLINGHAM, J. 2011 Drops climbing uphill on an oscillating substrate. *J. Fluid Mech.* **674**, 93–119.

BONN, D., EGGERS, J., INDEKEU, J., MEUNIER, J. & ROLLEY, E. 2009 Wetting and spreading. *Rev. Mod. Phys.* **81** (2), 739–805.

BRADSHAW, J. & BILLINGHAM, J. 2016 Thin three-dimensional droplets on an oscillating substrate with contact angle hysteresis. *Phys. Rev.* E **93** (1), 013123.

BRADSHAW, J. T. & BILLINGHAM, J. 2018 Thick drops climbing uphill on an oscillating substrate. *J. Fluid Mech.* **840**, 131–153.

BRUNET, P., EGGERS, J. & DEEGAN, R. D. 2007 Vibration-induced climbing of drops. *Phys. Rev. Lett.* **99** (14), 144501.

BRUNET, P., EGGERS, J. & DEEGAN, R. D. 2009 Motion of a drop driven by substrate vibrations. *Eur. Phys. J. Special Topics* **166** (1), 11–14.

DANIEL, S. & CHAUDHURY, M. K. 2002 Rectified motion of liquid drops on gradient surfaces induced by vibration. *Langmuir* **18** (9), 3404–3407.

DANIEL, S., SIRCAR, S., GLIEM, J. & CHAUDHURY, M. K. 2004 Ratcheting motion of liquid drops on gradient surfaces. *Langmuir* **20** (10), 4085–4092.

DARHUBER, A. A., VALENTINO, J. P., TROIAN, S. M. & WAGNER, S. 2003 Thermocapillary actuation of droplets on chemically patterned surfaces by programmable microheater arrays. *J. Microelectromech. Syst.* **12** (6), 873–879.

DATTILO, D., ARMELAO, L., FOIS, G., MISTURA, G. & MAGGINI, M. 2007 Wetting properties of flat and porous silicon surfaces coated with a spiropyran. *Langmuir* **23** (26), 12945–12950.

DING, H., ZHU, X., GAO, P. & LU, X. Y. 2018 Ratchet mechanism of drops climbing a vibrated oblique plate. *J. Fluid Mech.* **835**, R1.

DONG, L., CHAUDHURY, A. & CHAUDHURY, M. K. 2006 Lateral vibration of a water drop and its motion on a vibrating surface. *Eur. Phys. J.* E **21** (3), 231–242.

GLYCERINE PRODUCERS' ASSOCIATION 1963 Physical properties of glycerine and its solutions. Available at: http://www.aciscience.org/docs/physical_properties_of_glycerine_and_its_solutions. pdf).

JOHN, K. & THIELE, U. 2010 Self-ratcheting Stokes drops driven by oblique vibrations. *Phys. Rev. Lett.* **104** (10), 107801.

KEISER, A., KEISER, L., CLANET, C. & QUÉRÉ, D. 2017 Drop friction on liquid-infused materials. *Soft Matt.* **13** (39), 6981–6987.

LAFUMA, A. & QUÉRÉ, D. 2011 Slippery pre-suffused surfaces. *Europhys. Lett.* **96** (5), 56001.

LATIKKA, M., BACKHOLM, M., TIMONEN, J. V. I. & RAS, R. N. A. 2018 Wetting of ferrofluids: phenomena and control. *Curr. Opin. Colloid Interface Sci.* **36**, 118–129.

LIN, C. S., CHEN, S., XIAO, L. L. & LIU, Y. 2018 Tuning drop motion by chemical chessboard-patterned surfaces: a many-body dissipative particle dynamics study. *Langmuir* **34** (8), 2708–2715.

LIU, Q. C. & XU, B. X. 2015 Actuating water droplets on graphene via surface wettability gradients. *Langmuir* **31** (33), 9070–9075.

MISTURA, G. & PIERNO, M. 2017 Drop mobility on chemically heterogeneous and lubricant-impregnated surfaces. *Adv. Phys.* **2** (3), 591–607.

MUGELE, F. & BARET, J. C. 2005 Electrowetting: from basics to applications. *J. Phys.: Condens. Matter* **17** (28), R705–R774.

NAKAJIMA, A., NAKAGAWA, Y., FURUTA, T., SAKAI, M., ISOBE, T. & MATSUSHITA, S. 2013 Sliding of water droplets on smooth hydrophobic silane coatings with regular triangle hydrophilic regions. *Langmuir* **29** (29), 9269–9275.

NOBLIN, X., KOFMAN, R. & CELESTINI, F. 2009 Ratchetlike motion of a shaken drop. *Phys. Rev. Lett.* **102** (19), 194504.

RIGONI, C., FERRARO, D., CARLASSARA, M., FILIPPI, D., VARAGNOLO, S., PIERNO, M., TALBOT, D., ABOU-HASSAN, A. & MISTURA, G. 2018 Dynamics of ferrofluid drops on magnetically patterned surfaces. *Langmuir* **34** (30), 8917–8922.

SARTORI, P., BONATO, L., DELFITTO, G., PIERNO, M., MISTURA, G., SEMPREBON, C. & BRINKMANN, M. 2018 Morphological transitions of water channels induced by vertical vibrations. *Langmuir* **34** (43), 12882–12888.

SARTORI, P., QUAGLIATI, D., VARAGNOLO, S., PIERNO, M., MISTURA, G., MAGALETTI, F. & CASCIOLA, C. M. 2015 Drop motion induced by vertical vibrations. *New J. Phys.* **17**, 15.

SAVVA, N. & KALLIADASIS, S. 2013 Droplet motion on inclined heterogeneous substrates. *J. Fluid Mech.* **725**, 462–491.

SAVVA, N. & KALLIADASIS, S. 2014 Low-frequency vibrations of two-dimensional droplets on heterogeneous substrates. *J. Fluid Mech.* **754**, 515–549.

SBRAGAGLIA, M., BIFERALE, L., AMATI, G., VARAGNOLO, S., FERRARO, D., MISTURA, G. & PIERNO, M. 2014 Sliding drops across alternating hydrophobic and hydrophilic stripes. *Phys. Rev.* E **89** (1), 012406.

SCHELLENBERGER, F., XIE, J., ENCINAS, N., HARDY, A., KLAPPER, M., PAPADOPOULOS, P., BUTT, H.-J. & VOLLMER, D. 2015 Direct observation of drops on slippery lubricant-infused surfaces. *Soft Matt.* **11** (38), 7617–7626.

SEMPREBON, C., VARAGNOLO, S., FILIPPI, D., PERLINI, L., PIERNO, M., BRINKMANN, M. & MISTURA, G. 2016 Deviation of sliding drops at a chemical step. *Soft Matt.* **12** (40), 8268–8273.

SMITH, J. D., DHIMAN, R., ANAND, S., REZA-GARDUNO, E., COHEN, R. E., MCKINLEY, G. H. & VARANASI, K. K. 2013 Droplet mobility on lubricant-impregnated surfaces. *Soft Matt.* **9** (6), 1772–1780.

SOLVAY 2017 Fomblin pfpe lubes for vacuum applications. Available at: https://www.solvay.com/sites/g/files/srpend221/files/2018-10/Fomblin-PFPE-Lubes-for-Vaccum-Applications_EN-v2.7_0.pdf.

SUZUKI, S., NAKAJIMA, A., TANAKA, K., SAKAI, M., HASHIMOTO, A., YOSHIDA, N., KAMESHIMA, Y. & OKADA, K. 2008 Sliding behavior of water droplets on line-patterned hydrophobic surfaces. *Appl. Surf. Sci.* **254** (6), 1797–1805.

TÓTH, T., FERRARO, D., CHIARELLO, E., PIERNO, M., MISTURA, G., BISSACCO, G. & SEMPREBON, C. 2011 Suspension of water droplets on individual pillars. *Langmuir* **27** (8), 4742–4748.

VARAGNOLO, S., FERRARO, D., FANTINEL, P., PIERNO, M., MISTURA, G., AMATI, G., BIFERALE, L. & SBRAGAGLIA, M. 2013 Stick-slip sliding of water drops on chemically heterogeneous surfaces. *Phys. Rev. Lett.* **111** (6), 066101.

VARAGNOLO, S., SCHIOCCHET, V., FERRARO, D., PIERNO, M., MISTURA, G., SBRAGAGLIA, M., GUPTA, A. & AMATI, G. 2014 Tuning drop motion by chemical patterning of surfaces. *Langmuir* **30** (9), 2401–2409.

WONG, T. S., KANG, S. H., TANG, S. K. Y., SMYTHE, E. J., HATTON, B. D., GRINTHAL, A. & AIZENBERG, J. 2011 Bioinspired self-repairing slippery surfaces with pressure-stable omniphobicity. *Nature* **477** (7365), 443–447.

YEO, L. Y. & FRIEND, J. R. 2014 Surface acoustic wave microfluidics. *Annu. Rev. Fluid Mech.* **46**, 379–406.

ZHAO, J. Y., CHEN, S. & LIU, Y. 2016 Droplets motion on chemically/topographically heterogeneous surfaces. *Mol. Simul.* **42** (17), 1452–1459.

ZHAO, J. Y., CHEN, S. & LIU, Y. 2017 Dynamical behaviors of droplet impingement and spreading on chemically heterogeneous surfaces. *Appl. Surf. Sci.* **400**, 515–523.